

Warped Fermi Surface in GaSb from Shubnikov-de Haas Measurements*†

D. G. SEILER‡ AND W. M. BECKER

Department of Physics, Purdue University, Lafayette, Indiana 47907

(Received 20 February 1969)

The frequencies of Shubnikov-de Haas oscillations in n -type tellurium-doped GaSb have been obtained as a function of magnetic field direction in samples with electron concentrations $n \approx 10^{18} \text{ cm}^{-3}$. Field-modulation and phase-sensitive detection techniques were employed in the measurements. A frequency anisotropy of $\sim 1\%$ has been unambiguously determined. These results are explained by the warping contribution to the $k=0$ conduction-band energy expression derived by Kane using $\mathbf{k} \cdot \mathbf{p}$ perturbation theory. By fitting the frequency anisotropy to the theoretical prediction, it is found that the warping parameter $L-M-N = (11 \pm 2)\hbar^2/2m_0$. A small ($\sim 2\%$) effective-mass anisotropy has been observed; the symmetry of the result is predicted from the warping model, i.e., $m^*(111) > m^*(110) > m^*(100)$.

I. INTRODUCTION

CRYSTAL-GROWTH technology yields homogeneous single crystals of tellurium-doped n -type GaSb with carrier concentrations only between $\sim 10^{17}$ to $\sim 10^{18} \text{ cm}^{-3}$. Consequently, low-temperature galvanomagnetic measurements on these crystals involve carriers lying within a narrow energy range in the conduction band. For the concentrations 10^{17} – 10^{18} cm^{-3} , the E -versus- k relation is no longer parabolic, and the Fermi surface is expected to show departures from spherical symmetry. Thus, refined measurements may yield quite detailed information on the nature of the carriers at the Fermi surface, and experimental results may indeed serve as a test of E -versus- k theories. In turn, parameters of bands that are far distant in energy from the Fermi energy may be extracted from the data.

Because of the difficulty of making band-structure calculations from first principles, it is desirable to obtain information about band structure directly from experiment. The $\mathbf{k} \cdot \mathbf{p}$ method is probably one of the most important theoretical procedures for predicting and analyzing experimental parameters of the energy-band structures of semiconductors. Coupled with the use of symmetry, it shows that the band structure in the vicinity of a point in k space depends on a small number of parameters which may be determined by experiment. In this paper, we use an energy expression derived by the $\mathbf{k} \cdot \mathbf{p}$ method to obtain information about the band structure of GaSb.

The Shubnikov-de Haas (SdH) effect provides a sensitive method for examining details of the Fermi surface of metals and semiconductors. In n -GaSb(Te), observation of the SdH effect was first reported by Becker and Fan.¹ They ascribed the oscillatory behavior to conduction by carriers in the $k=0$ minimum. Their

observations of the damping of the oscillations were later shown² to be consistent with screening due to carriers in nearby subsidiary minima lying along $\langle 111 \rangle$ directions. Yep and Becker³ found a variation of the cyclotron-resonance effective mass with concentration from the analysis of the amplitude dependence of SdH oscillations in the same material. The interpretation of their results was based on Kane's "three-band approximation"⁴; higher-band $\mathbf{k} \cdot \mathbf{p}$ interactions were not considered. The nonparabolicity predicted from Kane's theory was shown to be in agreement with the experimental results when known values of the forbidden band energy gap E_g , the valence band spin-orbit splitting energy Δ , and a value of the momentum matrix element P consistent with values of this parameter found in other III-V compounds were employed in the calculation. In this paper we report results which indicate that the Fermi surface deviates from spherical symmetry; these deviations cannot be explained without considering the higher-band $\mathbf{k} \cdot \mathbf{p}$ interactions.

Earlier we had reported the observation of beating effects⁵ in the SdH oscillations of n -GaSb(Te) and had suggested that the beating effects might be ascribed to inversion asymmetry splitting of the $k=0$ conduction band. This suggestion was based on the remarkable similarity of our results to the observed beating effects in HgSe⁶ and on the theoretical arguments of Roth *et al.*⁷ explaining the HgSe data. More recently, we have reported that the SdH period exhibits a small, but reproducible, angular anisotropy.⁸ This anisotropy is consistent with a model of warping of the $k=0$ conduction band. In this paper, the detailed experimental results of our investigation are presented. The results are then compared with SdH frequency and cyclotron-resonance effective-mass values predicted on the basis of Kane's $\mathbf{k} \cdot \mathbf{p}$ perturbation theory. This comparison

* Work supported in part by the U. S. Army Research Office, Durham, and the Advanced Research Projects Agency.

† Based in part on a thesis submitted by D. G. Seiler to the Department of Physics, Purdue University, in partial fulfillment of the requirements for the degree of Doctor of Philosophy.

‡ Present address: Department of Physics, North Texas State University, Denton, Texas.

¹ W. M. Becker and H. Y. Fan, in *Proceedings of the International Conference on the Physics of Semiconductors, Paris, 1964* (Dunod Cie., Paris, 1965), p. 663.

² J. E. Robinson and S. Rodriguez, *Phys. Rev.* **135**, A779 (1964).

³ T. O. Yep and W. M. Becker, *Phys. Rev.* **144**, 741 (1966).

⁴ E. O. Kane, *J. Phys. Chem. Solids* **1**, 249 (1957).

⁵ D. G. Seiler and W. M. Becker, *Phys. Letters* **26A**, 96 (1967).

⁶ C. R. Whittett, *Phys. Rev.* **138**, A829 (1965).

⁷ L. M. Roth, S. H. Groves, and P. W. Wyatt, *Phys. Rev. Letters* **19**, 576 (1967).

⁸ D. G. Seiler and W. M. Becker, *Bull. Am. Phys. Soc.* **13**, 1455 (1968).

has enabled us to evaluate several of the higher-band parameters. Our investigation indicates that the observed angular anisotropy can be explained by warping alone, without recourse to consideration of inversion asymmetry splitting.

In Sec. II we summarize various features of the band structure of GaSb previously obtained by theoretical calculations and by experimental measurements. We present the theoretical expressions for the SdH effect in Sec. III A. Starting with an E -versus- k equation involving nonparabolicity and warping, expressions for the extremal cross-sectional area of the Fermi surface and cyclotron-resonance effective mass are derived in Secs. III B and III C. The experimental technique is described in Sec. IV. Details of data reduction are outlined in Sec. V. Finally, in Sec. VI, we present our results and show that they may be predicted on the basis of nonparabolicity and warping alone. In Appendix A, several angular functions are evaluated for various cases of interest. The values of the normalized coefficients a_4 , b_4 , and c_4 used in Kane's $\mathbf{k}\cdot\mathbf{p}$ perturbation theory are estimated in Appendix B. In Appendix C, we evaluate the higher-band parameter A' .

II. GaSb BAND STRUCTURE

Cohen and Bergstresser⁹ have calculated the energy-band structure of GaSb using a local pseudopotential model. More recently, Herman *et al.*¹⁰ carried out band-structure calculations utilizing the empirically adjusted OPW (orthogonalized plane-wave) method. Figure 1 shows the energy levels at the Γ point for their model. The lowest conduction band corresponds to antibonding s states with symmetry type Γ_1 . When the spin-orbit interaction is included, the conduction band has Γ_6 symmetry in the double group T_d^2 . The valence band has the symmetry given by bonding p functions and is of the symmetry type Γ_{15} . Adding the spin-orbit interaction removes the sixfold degeneracy at the Γ point. The split-off band with Γ_7 symmetry is separated from the fourfold degenerate Γ_8 bands by the spin-orbit splitting energy Δ . According to the calculations of Herman *et al.*, the Γ_{15} conduction band is separated from the top of the valence band by ~ 3.35 eV, which is somewhat smaller than the same band separation calculated by Cohen and Bergstresser. More recent estimates of the position of the Γ_{15} conduction band carried out by Zhang and Callaway¹¹ and by Higginbotham *et al.*¹² are in fair agreement with the results given in Ref. 10.

⁹ M. L. Cohen and T. K. Bergstresser, Phys. Rev. **141**, 789 (1966).

¹⁰ F. Herman, R. L. Kortum, C. D. Kuglin, J. P. Van Dyke, and S. Skillman, to be published in *Methods in Computational Physics*, edited by B. Adler, S. Fernbach, and M. Rotenberg (Academic Press Inc., New York, 1968), Vol. 8.

¹¹ H. I. Zhang and J. Callaway (to be published).

¹² C. W. Higginbotham, F. H. Pollak, and M. Cardona, in *Proceedings of the Ninth International Conference on the Physics of Semiconductors*, edited by S. M. Ryukin (Nauka Publishing House, Leningrad, 1968).

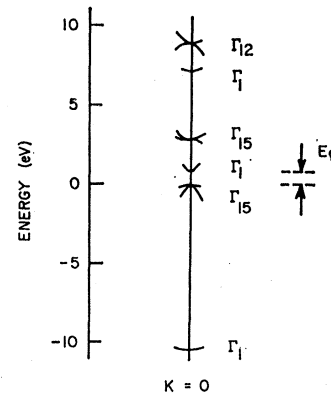


FIG. 1. Energy levels of GaSb at the Γ point according to Herman *et al.* (Ref. 10).

The understanding of transport phenomena involves knowledge of the features of the band structure at low carrier energies. In n -GaSb a variety of experimental determinations¹³⁻¹⁵ indicate that a two-conduction-band model is necessary to interpret experimental results. At low carrier concentrations and low temperatures, electrical conduction is by carriers in a band with a minimum at $k=0$. At higher temperatures and/or at higher carrier concentrations, conduction by carriers in germaniumlike subsidiary minima lying along $\langle 111 \rangle$ directions must be considered. Estimates of the energy separation between the $k=0$ minimum and the $\langle 111 \rangle$ valley edges are of the order 0.08–0.095 eV at 4.2°K.^{3,13-15} The electron concentration corresponding to the Fermi level position at the $\langle 111 \rangle$ band edge is $n \sim 1.25 \times 10^{18} \text{ cm}^{-3}$.

Sagar's¹³ study of the pressure and temperature dependence of the Hall coefficient and conductivity in GaSb indicated that the density-of-states ratio between the $\langle 111 \rangle$ valleys and the $k=0$ minimum is of the order 40. Studies by Becker, Ramdas, and Fan¹⁴ on the resistance, Hall coefficient, magnetoresistance, and optical absorption in crystals similar to those investigated by Sagar gave a density-of-states ratio as high as ~ 80 . The consequence of the large density-of-states ratio is that doping to high-impurity concentrations is ineffective in raising the Fermi energy much more than 0.01 eV above the $\langle 111 \rangle$ valley edge.

III. THEORETICAL ANALYSIS

A. Oscillatory Magnetoresistance

With the application of a magnetic field to a free-electron system, the motion in a plane perpendicular to the magnetic field becomes quantized and the quasicontinuous distribution of energy levels in the conduction band is split into highly degenerate Landau-

¹³ A. Sagar, Phys. Rev. **117**, 93 (1960).

¹⁴ W. M. Becker, A. K. Ramdas, and H. Y. Fan, J. Appl. Phys. Suppl. **32**, 2094 (1961).

¹⁵ H. B. Harland and J. C. Woolley, Ca. J. Phys. **44**, 2715 (1966).

level subbands. For each Landau level, the density of states is infinite at the bottom of the subband. The energy separation between the minima of adjacent Landau levels is equal to the cyclotron-resonance quantum of energy $\hbar\omega_c$; the n th Landau level lies a distance $(n+\frac{1}{2})\hbar\omega_c$ above the zero-field band edge, where n takes on positive integer values including zero. As the strength of the magnetic field increases, the energy separation between Landau levels becomes larger, so that these levels pass successively through the Fermi level. As a result, oscillations in transport properties (such as magnetoresistance and Hall effect) occur which are periodic in reciprocal magnetic field.

The following conditions are necessary for the oscillatory effects to be observed:

$$\omega_c\tau > 1, \quad (1)$$

where ω_c is the cyclotron-resonance frequency and τ is the carrier relaxation time;

$$\hbar\omega_c > k_B T, \quad (2)$$

where k_B is the Boltzmann constant and T is the temperature; and

$$\hbar\omega_c < E_F, \quad (3)$$

where E_F is the Fermi energy. This last condition places a limit on the maximum magnetic field beyond which no further oscillations would be seen. Above this limiting field, all the carriers are condensed into the $n=0$ Landau level.

The presence of a nonuniform distribution of ionized impurities in a crystal produces a spatial variation of the Fermi energy, and thus leads to a broadening of the Landau levels. A fourth requirement for the observation of oscillatory effects is that the Landau-level spacing should be much greater than the inhomogeneity broadening.

The period of oscillation P is related to the extremal cross-sectional area \mathcal{Q} of the Fermi surface by the expression¹⁶

$$P = 2\pi e / ch\mathcal{Q}, \quad (4)$$

where the quantities in Eq. (4) are given in MKS units.

A theory for the transverse magnetoconductivity oscillations for spherical energy surfaces has been given by Adams and Holstein for both acoustical lattice scattering and ionized impurity scattering.¹⁷ Using their theory, the oscillations in the transverse magnetoresistance can be expressed to a good approximation by

$$\frac{\Delta\rho}{\rho_0} = 5\sqrt{2}\pi^2 k_B \left(\frac{m^*c}{E_F e\hbar} \right)^{1/2} \frac{T}{B^{1/2}} \sum_{M=1}^{\infty} M^{1/2} (-1)^M \times \frac{e^{-M\beta T' m'/B} \cos(2\pi M/PB - \frac{1}{4}\pi) \cos \frac{1}{2} M\pi m'g}{\sinh(M\beta T m'/B)}, \quad (5)$$

¹⁶ J. M. Ziman, *Electrons and Phonons* (Oxford University Press, New York, 1960), p. 523.

¹⁷ E. N. Adams and T. D. Holstein, *J. Phys. Chem. Solids* **10**, 254 (1959).

where $\beta = 2\pi k_B m_0 c / e\hbar = 1.468 \times 10^5$ G/°K, $m' = m^*/m_0$ is the reduced effective mass, and g is the effective spectroscopic splitting factor. Here, ρ_0 is the zero-field resistivity, M denotes the M th harmonic of the oscillations, and T' is the nonthermal broadening temperature. The T' values determined from experiment may reflect both collision broadening and inhomogeneity broadening.¹⁸ The term $\cos \frac{1}{2} M\pi m'g$ takes into account the spin splitting of the Landau levels.¹⁹

In many instances, only the $M=1$ term is significant, since the higher harmonics ($M>1$) are severely damped at low fields. Thus, for most purposes

$$\Delta\rho/\rho_0 \approx -A_T(B) \cos(2\pi/PB + \varphi_0), \quad (6)$$

where

$$A_T(B) = 5\sqrt{2}\pi^2 k_B \left(\frac{m^*c}{E_F e\hbar} \right)^{1/2} \frac{T}{B^{1/2}} \frac{e^{-\beta T' m'/B} \cos \frac{1}{2} \pi m'g}{\sinh[\beta T m'/B]}, \quad (7)$$

and

$$\varphi_0 = -\frac{1}{4}\pi. \quad (8)$$

Low-frequency field modulation modifies the usual amplitude of the SdH oscillations by introducing a series of terms involving Bessel functions.^{20,21} The observed oscillatory signal can then be expressed as

$$\frac{\Delta\rho}{\rho_0} = -2A_T(B) \{ \cos(2\pi/PB + \varphi_0) [J_0(\alpha) + \sum_{n=1}^{\infty} (-1)^n J_{2n}(\alpha) \cos 2n\omega t] + \sin(2\pi/PB + \varphi_0) \times [\sum_{n=0}^{\infty} (-1)^n J_{2n+1}(\alpha) \cos(2n+1)\omega t] \}, \quad (9)$$

where $\alpha = 2\pi B_M / PB^2$ and B_M is the amplitude of the small ac magnetic field which varies at angular frequency ω . This series is reduced to a single term by using a lock-in amplifier detecting at a harmonic of the modulation frequency. For example, detection at the first harmonic of the modulation frequency reduces Eq. (9) to

$$\Delta\rho/\rho_0 = -2A_T(B) \sin(2\pi/PB + \varphi_0) J_1(\alpha), \quad (10)$$

and detecting at the second harmonic yields

$$\Delta\rho/\rho_0 = +2A_T(B) \cos(2\pi/PB + \varphi_0) J_2(\alpha). \quad (11)$$

The consequence of the Bessel-function modulation is that it reduces the signal amplitude at high fields and may introduce nodes at low fields, depending upon the amplitude of B_M relative to P .

¹⁸ K. F. Cuff, M. R. Ellett, and C. D. Kuglin, *J. Appl. Phys. Suppl.* **32**, 2179 (1961).

¹⁹ M. H. Cohen and E. I. Blount, *Phil. Mag.* **5**, 115 (1960).

²⁰ A. Goldstein, S. J. Williamson, and S. Foner, *Rev. Sci. Instr.* **36**, 1356 (1965).

²¹ B. L. Booth, Ph.D. thesis, Northwestern University, 1967 (unpublished).

B. Fermi Surface

Kane²² has used the $\mathbf{k}\cdot\mathbf{p}$ method to derive the approximate energy of the Γ_6 conduction band of the small-gap materials such as GaSb, InSb, InAs, and InP. His perturbation calculation yields

$$E_4^\pm = E_4' + u\hbar^2k^2/2m_0 + v f_1(\mathbf{k})\hbar^2/2m_0 \pm w f_2(\mathbf{k})\hbar^2/2m_0, \quad (12)$$

where

$$u = 1 + a_4^2 A' + b_4^2 M + c_4^2 L', \quad (13)$$

$$v = (b_4^2 - 2c_4^2)(L - M - N), \quad (14)$$

$$w = \sqrt{2}a_4 b_4 B', \quad (15)$$

$$f_1(\mathbf{k}) = (k_x^2 k_y^2 + k_x^2 k_z^2 + k_y^2 k_z^2)/k^2, \quad (16)$$

and

$$f_2(\mathbf{k}) = [k^2(k_x^2 k_y^2 + k_x^2 k_z^2 + k_y^2 k_z^2) - 9k_x^2 k_y^2 k_z^2]^{1/2}/k. \quad (17)$$

The conduction-band eigenvalue E_4' results from diagonalizing the Hamiltonian which includes the $\mathbf{k}\cdot\mathbf{p}$ and the largest spin-orbit interaction terms between an s -like (Γ_6) and p -like ($\Gamma_8 + \Gamma_7$) basis.

The normalized coefficient a_4 gives the amount of s -like basis function in the conduction-band eigenvector, and the normalized coefficients b_4 and c_4 give the amounts of different component p -like basis functions in the conduction-band eigenvector. The parameters A' , L , M , N , L' , and B' (Kane's B), written in units of $\hbar^2/2m_0$, represent the interaction between far-removed conduction and valence-band edges and the s - and p -like bands. The term $f_1(\mathbf{k})$ produces a warping of the Fermi surface and the term $f_2(\mathbf{k})$ gives the inversion asymmetry splitting.

E_4' depends on the magnitude of the Fermi-surface k vector. When the influence of higher-lying bands is neglected, E_4' is spherically symmetric. However, when the higher-lying band interactions are added, the magnitude of the k vector varies from point to point on the Fermi surface and E_4' is no longer spherically symmetric.²³

The secular equation for Kane's "three-band approximation"²² is

$$(E' - E_c)(E' - E_v)(E' - E_v + \Delta) - k^2 P^2 (E' - E_v + \frac{2}{3}\Delta) = 0, \quad (18)$$

where E' is the energy eigenvalue, Δ is the energy splitting of the valence band due to the spin-orbit interaction, and P is the momentum matrix element

$$- (i\hbar/m_0) \langle s | p_x | x \rangle.$$

If we take the energy zero at the top of the valence band, $E_v = 0$ and $E_c = E_g$, and Eq. (18) may be rewritten

as

$$(E' - E_g)(E') - k^2 P^2 \frac{E' + \frac{2}{3}\Delta}{E' + \Delta} = 0. \quad (19)$$

If we define $E_0' = E' - E_g$, then Eq. (19) can be rewritten in the form

$$E_0'^2 + E_g E_0' - k^2 P^2 (E_g + E_0' + \frac{2}{3}\Delta) / (E_g + E_0' + \Delta) = 0. \quad (20)$$

For GaSb, $E_0' \ll (E_g + \frac{2}{3}\Delta)$, and Eq. (20) becomes

$$E_0'^2 + E_g E_0' - k^2 P^2 (E_g + \frac{2}{3}\Delta) / (E_g + \Delta) = 0. \quad (21)$$

The solution corresponding to the conduction band eigenvalue E_4' is then

$$E_4' = -\frac{1}{2}E_g + \frac{1}{2}[E_g^2 + 4k^2 P^2 (E_g + \frac{2}{3}\Delta) / (E_g + \Delta)]^{1/2}, \quad (22)$$

where E_4' is the energy relative to the conduction-band minimum.

The possibility that warping in diamond and in zinc-blende semiconductors is sufficiently large to result in extremal cross-sectional areas away from $\mathbf{k}_H = 0$ (where \mathbf{k}_H is parallel to the magnetic-field direction) has been discussed by Roth *et al.*⁷ According to these authors, warping is found to vary slowly from material to material in these semiconductors. They calculate that warping three to six times larger than is estimated for these materials would be required to yield extremal cross-sectional areas away from $\mathbf{k}_H = 0$. Furthermore, recently observed beating effects⁵ in SdH oscillations in high-concentration n -type GaSb appear to be explainable by inversion asymmetry splitting of the conduction band and not by simple beating between an extremal area at $\mathbf{k}_H = 0$ and other extremal areas away from $\mathbf{k}_H = 0$. The warping that we observe in this experiment is very small (as predicted by Kane's model). Therefore, we conclude that the maximum cross-sectional area perpendicular to the magnetic field direction occurs at $\mathbf{k}_H = 0$.

Estimates of the magnitude of the inversion asymmetry splitting term in Eq. (12) have not yet been reported for GaSb. In this paper we present evidence that the inversion asymmetry term does not affect the period and hence does not interfere with any determination of the warping. Thus, for the purposes of this paper we can neglect the inversion asymmetry splitting term. In a subsequent paper we hope to report an analysis of beating effects in GaSb which will yield a value for the splitting term.

In calculating the extremal cross-sectional area of the Fermi surface, it is convenient to transform to the k components of a coordinate system in which \mathbf{B} is always parallel to one of the new coordinate axes. (The details of this transformation are given in Appendix A.) We substitute Eq. (22) into Eq. (12), and use

²² E. O. Kane, in *Semiconductors and Semimetals*, edited by R. K. Willardson and A. C. Beer (Academic Press Inc., New York, 1966), Vol. 1, p. 75.

²³ We thank Dr. Evan O. Kane for verifying this point.

the new coordinates given in Appendix A to obtain

$$E_4 = \frac{-E_g}{2} + \frac{E_g}{2} \left[1 + \frac{4k_\rho^2 P^2(E_g + \frac{2}{3}\Delta)}{E_g^2(E_g + \Delta)} \right]^{1/2} + \frac{u\hbar^2 k_\rho^2}{2m_0} + \frac{vy_1(\theta, \varphi)\hbar^2 k_\rho^2}{2m_0}, \quad (23)$$

where k_ρ and φ are a set of polar coordinates lying in the plane perpendicular to the magnetic field \mathbf{B} and θ is the angle between the field direction and a crystallographic direction lying in the plane of rotation of the magnetic field. (At this point, we drop the \pm notation, since we neglect the inversion asymmetry splitting term in any further calculations.) The form of the function $y_1(\theta, \varphi)$ depends on the plane of rotation of the magnetic field and is given in Appendix A for several cases of interest.

For the samples used in this investigation, the coefficients a_4 , b_4 , and c_4 , which are involved in the evaluation of u and v , are slowly varying functions of k_ρ^2 . Thus, a_4 , b_4 , and c_4 can be closely approximated by

$$k_\rho^2 = \frac{(E_4^2 + E_4 E_g) \left(1 + \frac{(2E_4 + E_g)v y_1(\theta, \varphi)}{P^2(E_g + \frac{2}{3}\Delta)/(E_g + \Delta)(\hbar^2/2m_0) + (2E_4 + E_g)u} \right)^{-1}}{P^2(E_g + \frac{2}{3}\Delta)/(E_g + \Delta) + \hbar^2(2E_4 + E_g)u/2m_0}. \quad (25)$$

Since

$$(2E_4 + E_g)v y_1(\theta, \varphi) \ll \frac{P^2(E_g + \frac{2}{3}\Delta)}{(E_g + \Delta)(\hbar^2/2m_0)} + (2E_4 + E_g)u,$$

Eq. (25) can be expanded to give

$$k_\rho^2 \approx C_0 [1 - C_1 y_1(\theta, \varphi)], \quad (26)$$

where

$$C_0 = (E_4^2 + E_4 E_g) /$$

$$\left[\frac{P^2(E_g + \frac{2}{3}\Delta)}{(E_g + \Delta)} + \hbar^2(2E_4 + E_g)u/2m_0 \right] \quad (27)$$

and

$$C_1 = (2E_4 + E_g)v /$$

$$\left[\frac{P^2(E_g + \frac{2}{3}\Delta)}{(E_g + \Delta)(\hbar^2/2m_0)} + (2E_4 + E_g)u \right]. \quad (28)$$

Thus the coefficients C_0 and C_1 are only dependent on the Fermi energy and the band parameters. When the k vector is along a $\langle 001 \rangle$ direction, $y_1(\theta, \varphi) = 0$; by Eq. (26), $C_0 = k_\rho^2(001)$, where $k_\rho(001)$ is the magnitude of the k vector in the $\langle 001 \rangle$ direction.

The extremal cross-sectional area \mathcal{A} perpendicular to the magnetic field is given by

$$\mathcal{A} = \frac{1}{2} \int_0^{2\pi} k_\rho^2(\theta, \varphi) d\varphi.$$

using an appropriate spherical radius vector k_F . In Appendix B we calculate values of E_4' , a_4 , b_4 , and c_4 as a function of k_F .

Rearranging Eq. (23) and squaring both sides of the resulting equation gives

$$\begin{aligned} E_4^2 + E_4 E_g + \frac{1}{4} E_g^2 - (2E_4 + E_g)(u + v y_1(\theta, \varphi)) \hbar^2 k_\rho^2 / 2m_0 \\ + [u + v y_1(\theta, \varphi)]^2 (\hbar^2 k_\rho^2 / 2m_0)^2 \\ = \frac{1}{4} E_g^2 + k_\rho^2 P^2(E_g + \frac{2}{3}\Delta) / (E_g + \Delta). \end{aligned} \quad (24)$$

The last term on the left-hand side of Eq. (24) is small compared to the other terms and hence can be neglected. Thus, Eq. (24) can be solved for k_ρ^2 , giving

Therefore, integrating Eq. (26), we get

$$\mathcal{A} = \pi C_0 [1 - (C_1/2\pi) g_1(\theta)], \quad (29)$$

where $g_1(\theta)$ is an integral defined in Appendix A. Using Eq. (4), the frequency of these oscillations is given by $F = \hbar \mathcal{A} / 2\pi e$. Thus, the frequency of the oscillations is

$$F(\theta) = (\hbar/2e) C_0 [1 - (C_1/2\pi) g_1(\theta)]. \quad (30)$$

C. Effective Mass

The cyclotron-resonance effective mass m^* can be expressed as²⁴

$$m^* = \frac{\hbar^2}{2\pi} \int_0^{2\pi} \frac{k_\rho d\varphi}{\partial E_4 / \partial k_\rho}. \quad (31)$$

For an accurate calculation of the cyclotron-resonance effective mass, E_4' can be written as

$$E_4' \approx \gamma E_g P^2 k_\rho^2 - \gamma^2 E_g P^4 k_\rho^4 + 2\gamma^3 E_g P^6 k_\rho^6, \quad (32)$$

where

$$\gamma = (E_g + \frac{2}{3}\Delta) / E_g^2 (E_g + \Delta). \quad (33)$$

(The term involving k_ρ^6 has been included in the energy expansion because of its non-negligible contribution to the effective mass.) Using Eq. (32) to evaluate $\partial E_4 / \partial k_\rho$,

²⁴ G. Dresselhaus, A. F. Kip, and C. Kittel, Phys. Rev. **98**, 368 (1955).

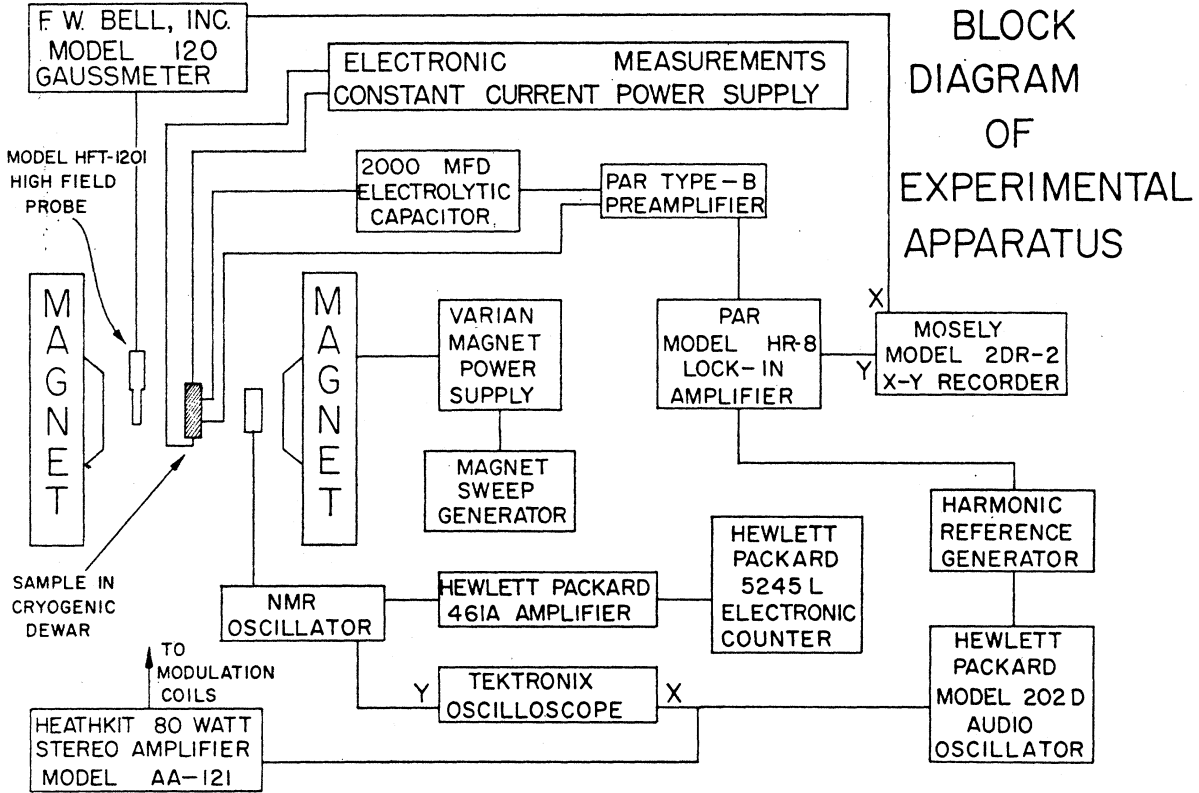


FIG. 2. Block diagram of the experimental apparatus.

Eq. (31) becomes

$$m^* = \frac{\hbar^2}{4\pi} \int_0^{2\pi} \frac{d\varphi}{[\gamma E_g P^2 - 2\gamma^2 E_g P^4 k_p^2 + 6\gamma^3 E_g P^6 k_p^4 + u\hbar^2/2m_0 + v\gamma_1(\theta, \varphi)\hbar^2/2m_0]} \quad (34)$$

Substituting expressions for k_p^2 and k_p^4 obtained from Eq. (26) into Eq. (34) and integrating, we get

$$m^* \cong \frac{1}{2} \hbar^2 K_0 [1 - (K_1/2\pi)g_1(\theta)], \quad (35)$$

where

$$K_0 = [\gamma E_g P^2 - 2\gamma^2 E_g P^4 C_0 + 6\gamma^3 E_g P^6 C_0^2 + u\hbar^2/2m_0]^{-1} \quad (36)$$

and

$$K_1 = \frac{2\gamma^2 E_g P^4 C_0 C_1 - 12\gamma^3 E_g P^6 C_0^2 C_1 + v\hbar^2/2m_0}{\gamma E_g P^2 - 2\gamma^2 E_g P^4 C_0 + 6\gamma^3 E_g P^6 C_0^2 + u\hbar^2/2m_0}. \quad (37)$$

In deriving Eq. (35), we have used the following approximations:

$$k_p^4 \approx C_0^2 [1 - 2C_1 y_1(\theta, \varphi)]$$

and

$$|K_1| \ll 1.$$

IV. EXPERIMENTAL

A. Sample Preparation

The single crystals of tellurium-doped n -type GaSb used in this investigation were grown by the Czochralski

technique. The ingot growth axis was either along a $\langle 111 \rangle$ or a $\langle 110 \rangle$ crystallographic direction. Oriented samples were taken from slices cut perpendicular to the ingot growth axis to reduce the effects of inhomogeneities.

B. Experimental Apparatus

Figure 2 shows a block diagram of the experimental apparatus. Magnetic fields up to 21.5 kG were made available using a 12-in. Varian electromagnet with poles tapered to $5\frac{1}{2}$ in. A 2000- μ F electrolytic capacitor was used to provide a high pass network, thus avoiding saturation of the transformer core in the type-B preamplifier by the dc component of the sample signal. To improve the impedance matching with the samples, the voltage transformation ratio of the transformer in the preamplifier was changed from the standard 100:1 ratio to a ratio of 350:1.

Magnetic field strengths were measured using NMR techniques. The NMR sample consisted of a solution of lithium chloride dissolved in water. It was found convenient to use the H^1 signal for field measurements below about 10 kG; the upper frequency limit of the

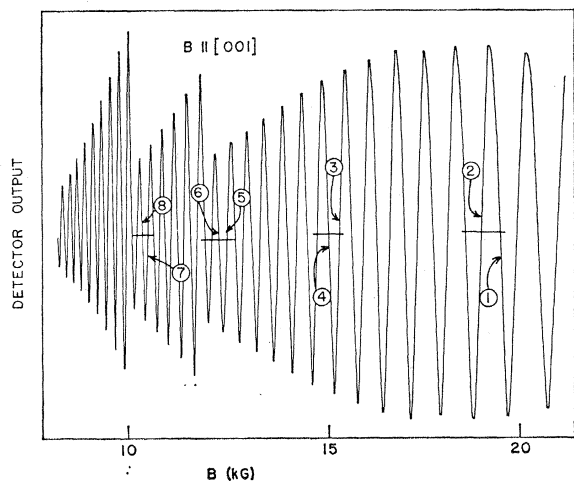


FIG. 3. Typical X-Y recorder data used for a period determination. Behavior shown is for sample 24B at 4.2°K. Adjustments in amplifier gain give the abrupt changes in oscillatory amplitude seen on the graph.

electronic counter required the use of the Li^7 signal for fields above 10 kG.

C. Period Measurement

An accurate period measurement involves a precise determination of the phase of the oscillations between two known magnetic fields. Melz has shown²⁵ that the magnetic field should be measured near a nodal point in the observed oscillations in order to minimize the uncertainty in the phase determination. Figure 3 shows typical oscillatory magnetoresistance data used for a period determination. The intersections of the horizontal bars with the detector output represent the positions of the observed nodal points. The vertical position of the bar corresponds to points midway between the maxima and minima amplitude envelopes. Points 1-8 represent the detector-signal positions at which the magnetic field strengths were determined. For each of these points, the field sweep was stopped during the measurement.

TABLE I. Sample properties and comparison of measured periods at 4.2 and 1.3°K. Periods are in units of 10^{-6} G^{-1} . θ is the magnetic field direction as shown in Figs. 4-6.

Sample	$R_{4.2^\circ\text{K}}$ (cm^2/C)	θ	Period 4.2°K	Period 1.3°K	$(P_{4.2} - P_{1.3})/P_{4.2}$
24B	-3.2	0°	2.4955	2.4945	+0.0004
		90°	2.4734	2.4724	+0.0004
		125°	2.4704	2.4682	+0.0009
58B	-3.8	+4°	2.5752	2.5721	+0.0012
		+49°	2.5962	2.5947	+0.0006
23B	-4.8				
80B	-5.0	95°	2.8187	2.8176	+0.0004
		134°	2.8169	2.8142	+0.0010
		189°	2.8395	2.8382	+0.0005

²⁵ P. J. Melz, Phys. Rev. 152, 540 (1966).

The oscillatory behavior is given by

$$A_0(B)\sin(2\pi/PB + \varphi_0),$$

where $A_0(B)$ is the observed oscillatory amplitude (which includes the influence of the Bessel function), P is the period, and φ_0 is the phase angle. Assuming φ_0 does not change with magnetic field, the period can then be found by determining the phase difference between a pair of points at which the NMR measurements of the field are made. Considering the four points 1, 2, 3, and 4 shown in Fig. 3, an average period of $(2.4949 \pm 0.0062) \times 10^{-6} \text{ G}^{-1}$ was obtained from period determinations between the pairs of points (1,3), (1,4), (2,3), and (2,4). An average period of $(2.4954 \pm 0.0027) \times 10^{-6} \text{ G}^{-1}$ was derived from period measurements between the pairs of points (3,5) (3,6), (4,5), and (4,6). The pairs of points (5,7), (5,8), (6,7), and (6,8) yielded an average period of $(2.4962 \pm 0.0009) \times 10^{-6} \text{ G}^{-1}$. The increase in error of the period with increasing field strength is attributable to distortion of the sinusoidal signal by higher-frequency SdH components. Within the precision of the measurements, no magnetic field dependence of the period was detected in the field range from 10-20 kG.

The data shown in Table I indicate that there is a slight but reproducible temperature dependence of the measured period. We attribute this small shift to the non-negligible contribution of the second-harmonic SdH term to the oscillatory behavior. The data on all samples were taken while detecting the sample signal at the first harmonic (fundamental) of the modulation frequency. Detecting the signal at the second harmonic of the modulation frequency amplifies the distortion of the oscillations caused by the presence of second and higher harmonics of the fundamental SdH frequencies. In fact, at $T=1.3^\circ\text{K}$ and for fields above 10 kG, the

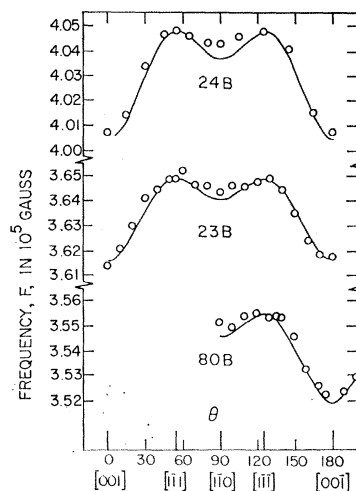


FIG. 4. Frequency of oscillations as a function of magnetic field direction with the magnetic field lying in a (110) plane. The smooth curves are calculated from Eq. (30) with the two parameters C_0 and C_1 adjusted to fit the experimental data (circles).

period measured by detecting the signal at the second harmonic of the modulation frequency can be as much as 1% lower than the period measured by detecting the signal at the first harmonic of the modulation frequency; below 10 kG this period difference becomes negligible. For $T=1.3^\circ\text{K}$ and second-harmonic detection of the signal, the influence of the second-harmonic SdH term can be directly seen in the asymmetry of the oscillatory behavior at high fields. For the three highest-concentration samples, data for the angular anisotropy determination were taken at 4.2°K to reduce further the harmonic distortion. For sample 80B, measurements were carried out at 1.3°K ; in this sample the damping was strong enough to make the higher-harmonic content insignificant in the field range of the measurements.

For angular positions close to the $\langle 111 \rangle$ magnetic field directions, previous measurements have revealed the presence of an amplitude minimum at ≈ 11 kG in sample 24B.⁵ Analysis of period data for this orientation was confined to fields well above 11 kG to avoid distortion occurring in the region of the minimum.

D. Amplitude Measurement

In separate measurements, the amplitudes of the oscillations were determined at 1.3 and 4.2°K . A time constant of one second was used throughout the measurements; the sweep speed of the dc magnetic field was adjusted so that the response of the lock-in amplifier did not lag behind the sample signal output.

V. EXPERIMENTAL DATA AND DATA REDUCTION

A. Frequencies

Figures 4 and 5 show the anisotropy of the frequency for samples of different carrier concentrations. The Hall

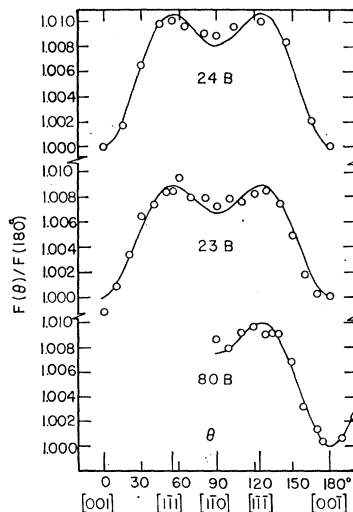


FIG. 5. Angular variation of the frequency ratio for B lying in a (110) plane. The curves show the one-parameter (C_1) least-squares fit of the data (circles) to Eq. (38).

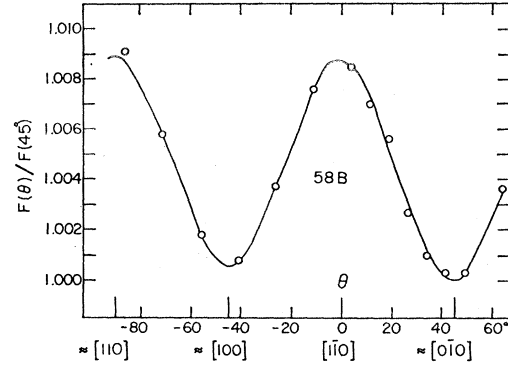


FIG. 6. Angular variation of the frequency ratio for B lying approximately in an (001) plane. The curve shows the one-parameter (C_1) least-squares fit of the data (circles) using the angular function $g_1(\theta)$ given in Eq. (A8).

coefficients of the samples used in this investigation are listed in Table I. The solid lines in the figures represent the values of the frequencies predicted by Eq. (30) using experimentally determined values of C_0 and C_1 and the expression for $g_1(\theta)$ given by Eq. (A5). For each sample, a value of C_1 was given by a one-parameter least-squares fit to the frequency ratio $F(\theta)/F(180^\circ)$, where

$$\frac{F(\theta)}{F(180^\circ)} = \frac{[1 - C_1 g_1(\theta)/2\pi]}{[1 - C_1 g_1(180^\circ)/2\pi]}, \quad (38)$$

where $F(\theta)$ is defined by Eq. (30). Using the experimental value of $F(\theta)$ in the field direction $\mathbf{B} \parallel [1\bar{1}\bar{1}]$ and the respective value of C_1 previously determined, Eq. (30) was solved for C_0 . Figure 6 shows a plot of the ratio $F(\theta)/F(45^\circ)$ as a function of magnetic field direction with B lying approximately in a (001) plane. The solid line shows the one-parameter least-squares fit to the data points assuming a $g_1(\theta)$ given by Eq. (A8). For this sample (58B) the current direction was 8° away from the $[001]$ direction; the appropriate transformation is given in part II of Appendix A. The results of our fitting procedure are shown in Table II. SHARE program No. 3094 was used to compute the least-squares estimation of C_1 .

B. Effective Masses

The effective-mass determination necessitates measurement of the amplitude of the SdH oscillations at different temperatures, and a comparison of the amplitude ratio at fixed fields to the theoretical ampli-

TABLE II. Experimental values of C_0 and C_1 .

Sample	C_0 in units of $eV/(\hbar^2/2m_0)$	C_1
24B	0.0045896	-0.086
58B	0.0044084	-0.093
23B	0.0041512	-0.072
80B	0.0040354	-0.081

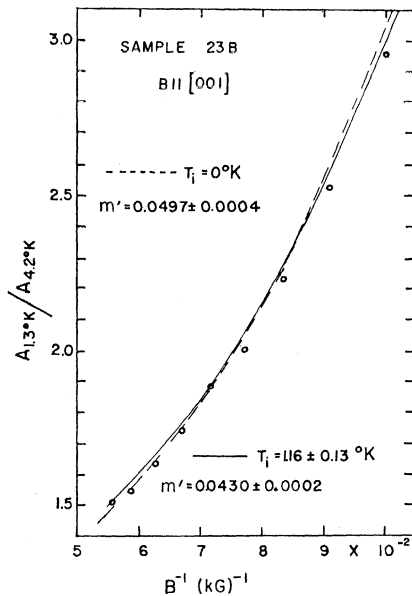


FIG. 7. Ratio of the oscillatory amplitudes as a function of reciprocal magnetic field for sample 23B. The solid line represents a two-parameter least-squares fit of the experimental data (circles) to Eq. (40), giving $T_i = 1.16 \pm 0.13^\circ\text{K}$ and $m' = 0.0430 \pm 0.0002$. The dashed line is calculated from Eq. (39) assuming $T_i = 0^\circ\text{K}$ and $m' = 0.0497 \pm 0.0004$.

tude. Typical amplitude data are shown in Fig. 7. Since the effective-mass determination is very sensitive to the inclusion or omission of possible damping terms in the theoretical SdH amplitude, we consider two cases of interest: (i) $T_i = 0$, that is, no inhomogeneity broadening; and (ii) $T_i \neq 0$.

(i) $T_i = 0$. Assuming T' is independent of temperature and considering only the $M = 1$ contribution to the SdH amplitude, Eq. (7) can be used to express the ratio of oscillatory amplitudes as

$$\frac{A_{T_1}}{A_{T_2}} = \frac{T_1 \sinh(\beta m' T_2/B)}{T_2 \sinh(\beta m' T_1/B)}. \quad (39)$$

Using the amplitude data taken at 1.3 and 4.2°K, Eq. (39) was solved for m' at various values of B , for data with $\mathbf{B} \parallel \langle 001 \rangle$, $\mathbf{B} \parallel \langle 1\bar{1}0 \rangle$, and $\mathbf{B} \parallel \langle 1\bar{1}1 \rangle$. No significant variation of m' with magnetic field could be found in the field range 9–18 kG. The average values of m' over this field range and their average deviation are listed in Table III.

(ii) $T_i \neq 0$. Hinkley and Ewald²⁶ have treated the damping introduced by sample inhomogeneity in their studies of grey tin by substituting $(T + T_i)$ for T , where T_i is defined as the inhomogeneity broadening temperature. Also, in their analysis T' is replaced by T_D , the Dingle broadening temperature. An empirical justification for this treatment has been given by Booth and

Ewald²⁷ in a subsequent study on the same material. Following Booth and Ewald, we may write A_{T_1}/A_{T_2} as

$$\frac{A_{T_1}}{A_{T_2}} = \frac{(T_1 + T_i) \sinh[\beta m' (T_2 + T_i)/B]}{(T_2 + T_i) \sinh[\beta m' (T_1 + T_i)/B]}, \quad (40)$$

under the assumption that T_i and T_D are independent of temperature. Using Eq. (40), we have calculated pairs of values of m' and T_i from the experimentally determined ratios $A_{1.3^\circ\text{K}}/A_{4.2^\circ\text{K}}$, by using a two-parameter least-squares fit to these ratios at various values of the magnetic field. The results and the standard error found from the computer program are shown in Table IV.

C. Phase Angles

According to Hinkley and Ewald,²⁶ the condition for a node to occur is

$$2\pi/PB_n + \varphi_0 + \pi = (2n + \frac{1}{2})\pi, \quad (41)$$

where n takes on both integer and half-integer values. The usual method of finding φ_0 involves plotting the positions of the nodal points versus integers, and the value of φ_0 is then obtained from the intercept at infinite field. In our measurements the magnetic field was usually not measured exactly at a nodal point. At any particular magnetic field B ,

$$2\pi/PB + \varphi_0 + \pi = (2n + \frac{1}{2})\pi + \Phi, \quad (42)$$

where Φ is now the oscillatory phase difference between the nodal position given by B_n and the position at which the field B was measured. The phase difference Φ is found directly from the recorder data. Since the actual data were taken while detecting at the first harmonic of the modulation frequency, the resultant detector output represents the first derivative of the unmodulated oscillatory effect. Thus, a node in the dc signal is seen as an antinode when detecting at the first harmonic. In the analysis, the n values are chosen so that φ_0 is restricted to the range

$$-\pi < \varphi_0 < 0. \quad (43)$$

Several values of φ_0 for each field direction were calculated by using the points (for example, points 1–8 in Fig. 3) where the field sweep was stopped. Thus, the values of φ_0 shown in Fig. 8 represent an average value of φ_0 over the magnetic field range of the measurement.

TABLE III. Reduced effective masses calculated with the assumption $T_i = 0$.

Sample	$m'(\bar{1}\bar{1}1)$	$m'(\bar{1}\bar{1}0)$	$m'(001)$
24B	0.0533 ± 0.0004	0.0526 ± 0.0002	0.0521 ± 0.0003
23B	0.0506 ± 0.0006	0.0501 ± 0.0004	0.0497 ± 0.0004

²⁶ E. D. Hinkley and A. W. Ewald, Phys. Rev. **134**, A1261 (1964).

²⁷ B. L. Booth and A. W. Ewald, Phys. Rev. Letters **18**, 491 (1967).

VI. RESULTS AND DISCUSSION

The results of the period measurements give a clear indication that the $k=0$ conduction-band energy surface is warped. Although the frequency anisotropy is extremely small, the observed frequency anisotropy in Figs. 3–5 are both predictable from the function $g_1(\theta)$ referred to the appropriate plane of rotation of the magnetic field. The sign and absolute value of the parameter C_1 , respectively, characterize the symmetry and magnitude of the observed frequency anisotropy. The values of C_1 obtained for three samples with \mathbf{B} lying in the (110) plane, and a value of C_1 for a sample with \mathbf{B} lying near the (001) plane, are not very different from one another. As will be described below, the parameter C_1 is not expected to be too sensitive to changes in Fermi-level position for the concentration range corresponding to the samples listed in Table II. A further verification of the warping model is that the experimentally determined effective mass is largest in the $\langle 1\bar{1}1 \rangle$ directions and smallest in the $\langle 001 \rangle$ directions, as predicted from Eq. (35). Although the error of each separate mass determination is of the same order of magnitude as the mass anisotropy, the consistency in results for the two samples listed in Tables III and IV indicates that the mass anisotropy is real.

The experimental value of C_1 can be used to estimate a value of $L-M-N$, the higher-band parameter which determines the amount of warping. This parameter is defined as follows²²:

$$L-M-N \equiv 3G - 2H_1, \quad (44)$$

where

$$H_1 = \frac{2}{m_0} \sum_j \frac{\Gamma_{15}}{E_v - E_j} |\langle x | p_y | u_j \rangle|^2 \quad (45)$$

and

$$G = \frac{1}{m_0} \sum_j \frac{\Gamma_{12}}{E_v - E_j} |\langle x | p_x | u_j \rangle|^2. \quad (46)$$

The summation in H_1 is over all states u_j transforming like Γ_{15} and the summation in G is over all states u_j transforming like Γ_{12} .²⁸ E_v is the energy of the Γ_{15}

TABLE IV. Reduced effective masses and inhomogeneity temperatures calculated with the assumption $T_i \neq 0$.

Sample	Field direction	m'	T_i , °K
24B	$\langle 1\bar{1}1 \rangle$	0.0474 ± 0.0007	1.28 ± 0.72
	$\langle 1\bar{1}0 \rangle$	0.0469 ± 0.0006	1.31 ± 0.77
	$\langle 001 \rangle$	0.0466 ± 0.0008	1.40 ± 1.06
23B	$\langle 1\bar{1}1 \rangle$	0.0441 ± 0.0007	0.84 ± 0.20
	$\langle 1\bar{1}0 \rangle$	0.0433 ± 0.0007	1.00 ± 0.17
	$\langle 001 \rangle$	0.0430 ± 0.0002	1.16 ± 0.13

²⁸ The higher-band parameters will be used as dimensionless quantities and must be multiplied by $\hbar^2/2m_0$ to equal parameters with the same symbols as in Ref. 22.

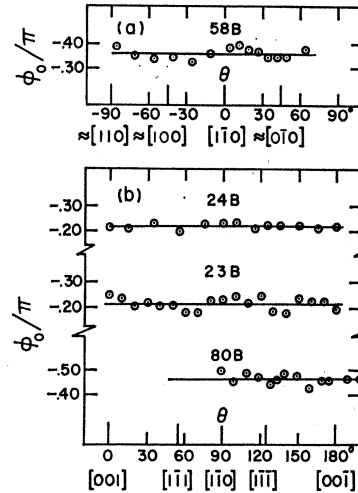


Fig. 8. Angular variation of the phase factor φ_0/π for (a) sample 58B with magnetic field lying in an approximate (001) plane, and (b) samples 80B, 23B, and 24B, with magnetic field lying in a (110) plane.

state at the top of the valence band; p_x , p_y , and p_z are the components of the momentum operator; and x , y , and z are functions that have the symmetry of the atomic p functions x , y , and z under the operations of the tetrahedral group.

The one-parameter least-squares fit to the experimental frequency ratios yields negative values for C_1 . Using Eq. (28), we note that the sign of C_1 is given by the sign of v . The sign and magnitude of v depends on the product $(b_4^2 - 2c_4^2)(L - M - N)$, according to Eq. (14). The quantity $(b_4^2 - 2c_4^2)$ is always negative for the assumed values of the band parameters (E_g , Δ , and P), as can be seen from Appendix B. A negative value for C_1 therefore implies that $L - M - N > 0$. Equation (28) can then be used to determine v (or $L - M - N$) if the experimental value of C_1 and known values of E_4 and u are employed in the calculation. If E_4 is known and the experimental value of C_0 is used, Eq. (27) then yields a value for u . The value of E_4 is not known precisely; previous measurements indicate that, in a sample with a carrier concentration similar to that of sample 80B, the Fermi energy is at the band edge of the $\langle 111 \rangle$ valleys. Estimates of this energy range from 0.08–0.095 eV. We use this energy range to determine the range in u and v (and hence in $L - M - N$). If u is known, then it is also possible to calculate the higher-band parameter A' . This calculation is carried out in Appendix C. A band-gap energy E_g of 0.81 eV, a spin-orbit splitting energy $\Delta = 0.80$ eV, and a value for $P = 9.48 \times 10^{-8}$ eV cm will be assumed in evaluating u and in all further computations. The values of E_g and Δ are given by Long.²⁹ We use a value of P estimated by Yep³⁰ and

²⁹ D. Long, in *Semiconductors and Semimetals*, edited by R. K. Willardson and A. C. Beer (Academic Press Inc., New York, 1966), Vol. 1, p. 143.

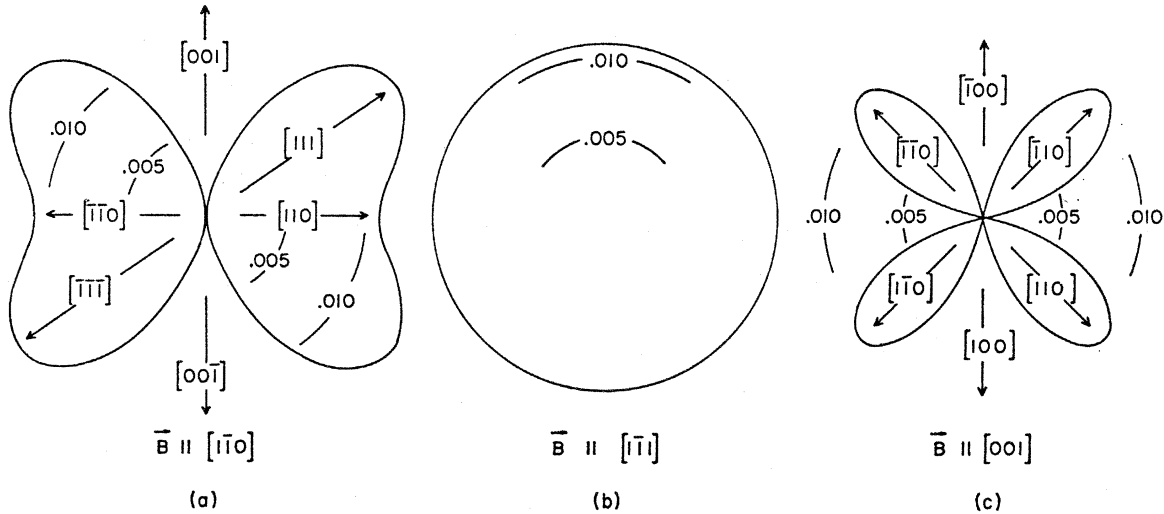


FIG. 9. Polar plots of $\chi = [k_p(\varphi) - k_p(001)]/k_p(001)$ for (a) $\theta = 90^\circ$, (b) $\theta = 55^\circ$, and (c) $\theta = 0^\circ$, assuming $C_1 = -0.086$. The scale markings indicate the magnitude of χ .

Becker³ from earlier results of Zwerdling *et al.*³⁰ Using a Fermi energy of 0.08 eV and the experimental values of C_0 and C_1 for sample 80B gives $u = -2.1$ and $v = -1.49$. Evaluation of b_4 and c_4 for sample 80B by the method outlined in Appendix B gives $b_4^2 - 2c_4^2 = -0.144$; thus $L - M - N = +10.3$. A choice of $E_4 = 0.095$ eV yields $u = +1.7$. The matrix-element sums A' , M , and L' are all negative; therefore u is restricted to values less than +1. For $u = +1$, Eq. (27) yields an upper limit of $E_4 \approx 0.092$ eV, using the C_0 value of sample 80B. This choice of E_4 gives $L - M - N = +11.9$. Thus, an error estimate based on the uncertainty in E_4 and the corresponding uncertainty in u leads to $+10.3 < L - M - N < +11.9$. We estimate an additional error of $\sim 10\%$ in $L - M - N$ from the scatter in the values of C_1 in Table II. Thus, $L - M - N = 11 \pm 2$, in units of $\hbar^2/2m_0$.

Cyclotron-resonance results in Ge²⁴ give positive values for $L - M - N$. In InSb, cyclotron-resonance results³¹ and measurements of the Burstein shift³² indicate positive values for the same quantity. Stradling³³ has obtained cyclotron-resonance effective-mass results for *p*-GaSb. For the heavy hole masses he finds $m_{111}^* = (0.36 \pm 0.03)m_0$ and $m_{100}^* = (0.26 \pm 0.04)m_0$. In order to obtain an estimate of the value of $L - M - N$ from these results, we will use an approximate expression for the heavy-mass band which has been given by Kane.²² Kane's result may be expressed in the following form:

$$E_3 = \alpha k^2 [1 + \gamma(k_x^2 k_y^2 + k_y^2 k_z^2 + k_z^2 k_x^2)/k^4], \quad (47)$$

where

$$\alpha = (1 + M)\hbar^2/2m_0 \quad (48)$$

and

$$\gamma = (L - M - N)/(1 + M). \quad (49)$$

³⁰ S. Zwerdling, B. Lax, K. Button, and L. M. Roth, *J. Phys. Chem. Solids* **9**, 320 (1959).

³¹ D. M. S. Bagguley, M. L. A. Robinson, and R. A. Stradling, *Phys. Letters* **6**, 143 (1963).

³² G. W. Gobeli and H. Y. Fan, *Phys. Rev.* **119**, 613 (1960).

³³ R. A. Stradling, *Phys. Letters* **20**, 217 (1966).

It can be shown³⁴ that

$$m^*(001) = -(\hbar^2/2\alpha)(1 + \frac{1}{4}\gamma)^{-1/2} \quad (50)$$

and

$$m^*(111) = -(\hbar^2/2\alpha)(1 + \frac{1}{4}\gamma)^{-1}. \quad (51)$$

Using Stradling's results, Eqs. (50) and (51) can be solved to give $\alpha = -5.3$ (in units of $\hbar^2/2m_0$) and $\gamma = -1.9$. By Eq. (48), $M = -6.3$ and, by Eq. (49), $L - M - N \approx +10$. If Stradling's error limits on the effective-mass data are taken into account, the analysis yields $-9.1 < M < -4.7$, and $+2.5 < L - M - N < +22$. Our results fall well within the range of values of $L - M - N$ expected from this analysis of Stradling's data.

Our model may be used to estimate the expected change of C_1 with Fermi energy. Choosing $E_4 = 0.085$ eV for sample 80B gives a value of $E_4 = 0.096$ eV for sample 24B using Eq. (27) and the experimental values of C_0 . The data of sample 80B and the choice $E_4 = 0.085$ eV then yield a value of $L - M - N = +11.0$. For this value of $L - M - N$, $C_1 \approx -0.095$ for sample 24B. Considering the error in the measurement, the values of C_1 for the samples investigated are consistent with this estimated variation in C_1 with Fermi energy.

The quantity $b_4^2 - 2c_4^2$ (and thus C_1) approaches zero with decreasing Fermi energy. The angular anisotropy of the period would therefore be expected to disappear in low-concentration samples. Because of the sharp increase in damping of the oscillations as the Fermi level falls below the $\langle 111 \rangle$ band edge, precise measurements of the period become increasingly more difficult for decreasing n when $n \lesssim 10^{18} \text{ cm}^{-3}$. Sample 80B represents a practical limit for observation of the angular anisotropy of the SdH frequency in GaSb for the

³⁴ H. T. Tohver, Ph.D. thesis, Purdue University, 1968 (unpublished).

measurement technique described in this paper. The symmetry of the conduction band in InSb is the same as that in GaSb. The quantity $b_4^2 - 2c_4^2$ would therefore be expected to fall to zero with decreasing concentration in InSb. In *n*-InSb, de Haas-van Alphen measurements by Sladek *et al.*³⁵ indeed seem to indicate that the angular anisotropy of the extremal cross-sectional area at $\mathbf{k}_H=0$ decreases as the carrier concentration is lowered. In contrast, the magnitude of the angular anisotropy observed by Booth and Ewald on grey tin³⁶ does not change appreciably for a wide range of carrier concentrations. This latter result is expected for a band of Γ_8 symmetry.

Departures of the Fermi surface from sphericity due to warping only may be obtained from Eq. (26) and experimental values of C_1 . We define as an index of deviation from sphericity the quantity $\chi = [k_\rho(\varphi) - k_\rho(001)]/k_\rho(001)$, where $k_\rho(\varphi) \approx C_0^{1/2}[1 - \frac{1}{2}C_1 y_1(\theta, \varphi)]$ for a given θ . In this approximation $\chi \approx -\frac{1}{2}C_1 y_1(\theta, \varphi)$. Plots of χ for the $k=0$ conduction band of GaSb are shown in Fig. 9. As expected for a warping model, the Fermi surface protrudes out in the $\langle 111 \rangle$ directions. Looking at Fig. 9, one can see immediately that the extremal cross-sectional area is largest for $\mathbf{B} \parallel [1\bar{1}1]$ and smallest for $\mathbf{B} \parallel [001]$.

Our effective-mass data gives negative values for K_1 in Eq. (35). This result is predicted from Eq. (37) using the experimentally determined C_0 and C_1 values for the two samples investigated and employing the estimates of the band parameters discussed previously. For these samples, the calculated magnitude of K_1 is approximately equal to the magnitude of C_1 , as expected. The effective-mass values given in Tables III and IV are consistent with previous determinations.^{3,14,30,37} The difference between the effective-mass values listed in Tables III and IV shows that the effective mass is greatly affected by the inclusion or omission of possible damping terms in the theoretical SdH amplitude.

The period measurement employed in this study did not require a measurement of the phase φ_0 , defined in Eq. (6). However, the precision of the period measurement allows a much more accurate phase determination than has been heretofore reported. We have therefore exploited the measurements technique to investigate the possible magnitude of variation of φ_0 with field direction. As seen in Fig. 8, no systematic angular variation of φ_0 is detectable. The phase is theoretically equal to $-\frac{1}{4}\pi$. For samples 23B and 24B, the phase is close to this value, whereas, for samples 80B and 58B, the phase is significantly higher than the theoretical prediction.

The theoretical derivation presented in this paper is directly applicable to the analysis of de Haas-van

Alphen-like data in other semiconductors with conduction bands described by Eq. (12). The approximations in the theory required for each semiconductor would be expected to lead to the appropriate functional forms for C_0 and C_1 . Evidence for angular variation of the extremal cross-sectional area in InSb has been obtained from de Haas-van Alphen data.³⁵ In the same material, SdH measurements at high electron concentrations show an angular variation of the SdH frequency.³⁸ Both sets of results may be shown to be consistent with the warping model presented in this paper.³⁹

ACKNOWLEDGMENTS

The authors acknowledge many helpful discussions with Dr. H. T. Tohver and the many numerical computations performed by R. A. Metzler. We also wish to thank Miss Louise Roth for growing the single crystals and Professor H. J. Yearian for orienting the samples.

APPENDIX A

In this appendix we outline the transformation of k coordinates from a crystallographic coordinate system (k_x, k_y, k_z axes along the crystallographic axes) to a new coordinate system in which one coordinate axis is along the magnetic field direction. The function $f_1(\mathbf{k})$ appearing in Eq. (12) is transformed into coordinate systems corresponding to experiment; the resulting transformation is then expressed in terms of polar coordinates. The angular function $y_1(\theta, \varphi)$ which appears as a result of the transformation is presented next. Finally, we perform an angular integration to give

$$g_1(\theta) = \int_0^{2\pi} y_1(\theta, \varphi) d\varphi,$$

the function required in the frequency analysis.

I. B Lying in a (110) Plane

We start with a crystallographic coordinate system k_x, k_y, k_z . A clockwise rotation about the k_z axis through an angle $\gamma (=45^\circ)$ gives a new coordinate system k_x', k_y', k_z' . Next, a counterclockwise rotation through an angle θ about the k_y' axis defines the coordinate system k_x'', k_y'', k_z'' . Thus, the transformation equations are

$$\begin{aligned} k_x &= k_x'' \cos\theta \cos\gamma + k_y'' \sin\gamma + k_z'' \sin\theta \cos\gamma, \\ k_y &= -k_x'' \cos\theta \sin\gamma + k_y'' \cos\gamma - k_z'' \sin\theta \sin\gamma, \\ k_z &= -k_x'' \sin\theta + k_z'' \cos\theta. \end{aligned} \quad (\text{A1})$$

If the magnetic field is parallel to the k_z'' axis, then θ is the angle between the magnetic field and the k_z axis. We set $k_x''=0$, since we assume that the extremal

³⁵ R. J. Sladek, A. S. Joseph, and E. R. Gertner, Phys. Letters **27A**, 504 (1968).

³⁶ B. L. Booth and A. W. Ewald, Phys. Rev. **168**, 805 (1968).

³⁷ H. Piller, J. Phys. Chem. Solids **24**, 425 (1963).

³⁸ G. A. Antcliffe and R. A. Stradling, Phys. Letters **20**, 119 (1966).

³⁹ R. J. Sladek, D. G. Seiler, A. S. Joseph, and E. R. Gertner (to be published).

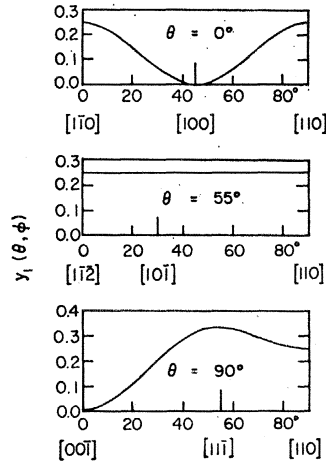


FIG. 10. Plots of $y_1(\theta, \varphi)$ versus φ , for $\theta=0^\circ$, $\theta=55^\circ$, and $\theta=90^\circ$ for \mathbf{B} lying in the (110) plane.

cross-sectional area occurs in the plane $k_z''=0$. Letting $\gamma=45^\circ$ and introducing the polar coordinates k_ρ and φ , where $k_x''=k_\rho \cos \varphi$ and $k_y''=k_\rho \sin \varphi$, Eqs. (A1) become

$$\begin{aligned} k_x &= (1/\sqrt{2})(\cos \theta \cos \varphi + \sin \varphi)k_\rho, \\ k_y &= (1/\sqrt{2})(-\cos \theta \cos \varphi + \sin \varphi)k_\rho, \\ k_z &= -(\sin \theta \cos \varphi)k_\rho. \end{aligned} \quad (\text{A2})$$

Substituting Eqs. (A2) into Eq. (16), we get the result

$$f_1(\mathbf{k}) = k_\rho^2 y_1(\theta, \varphi), \quad (\text{A3})$$

where

$$y_1(\theta, \varphi) = \frac{1}{4}[\cos^4 \varphi (-3 - 3 \cos^4 \theta + 10 \cos^2 \theta) + 2 \cos^2 \varphi (1 - 3 \cos^2 \theta) + 1]. \quad (\text{A4})$$

Integration yields

$$g_1(\theta) = \int_0^{2\pi} y_1(\theta, \varphi) d\varphi = \frac{\pi}{16}[8 - (-1 + 3 \cos^2 \theta)^2]. \quad (\text{A5})$$

$$\begin{aligned} y_1(\theta, \varphi) &= \{ \cos^4 \varphi [(-\sin \theta \cos \alpha + \cos \theta \sin \alpha)^2 (\sin \theta \sin \alpha + \cos \theta \cos \alpha)^2 + (\sin \theta \sin \alpha + \cos \theta \cos \alpha)^4 \sin^2 \beta \cos^2 \beta] \\ &\quad + \cos^2 \varphi \sin \varphi [2(\sin \theta \sin \alpha + \cos \theta \cos \alpha)^3 \sin \beta \cos \beta (\cos^2 \beta - \sin^2 \beta)] + \cos^2 \varphi \sin^2 \varphi [(-\sin \theta \cos \alpha + \cos \theta \sin \alpha)^2 \\ &\quad + (\sin \theta \sin \alpha + \cos \theta \cos \alpha)^2 (\cos^4 \beta - 4 \sin^2 \beta \cos^2 \beta + \sin^4 \beta)] \\ &\quad + \cos \varphi \sin^3 \varphi [2(\sin \theta \sin \alpha + \cos \theta \cos \alpha) \sin \beta \cos \beta (\sin^2 \beta - \cos^2 \beta)] + \sin^4 \varphi \sin^2 \beta \cos^2 \beta \}. \end{aligned} \quad (\text{A7})$$

Setting $\alpha=45^\circ$ and $\beta=8^\circ$ and integrating, we find that

$$\begin{aligned} g_1(\theta) &= [(-\sin \theta + \cos \theta)^2 (\sin \theta + \cos \theta)^2 + (\sin \theta + \cos \theta)^4 \\ &\quad \times (0.01899)] \left[\frac{3}{16} \pi \right] + [(-\sin \theta + \cos \theta)^2 \\ &\quad + (\sin \theta + \cos \theta)^2 (0.88606)] \left[\frac{3}{8} \pi \right] + 0.01424 \pi. \end{aligned} \quad (\text{A8})$$

APPENDIX B

In this appendix, values of E_4' , a_4 , b_4 , and c_4 are calculated as a function of the radius k_F of a spherical Fermi surface.

Equation (19) may be rewritten in the form

$$E'^3 + pE'^2 + qE' + r = 0, \quad (\text{B1})$$

Plots of $y_1(\theta, \varphi)$ for $\theta=0^\circ$, 55° , and 90° for \mathbf{B} lying in the (110) plane are given in Fig. 10. Results for $g_1(\theta)$ in the three principal directions are then given by Eq. (A5): $g_1(001) = \frac{1}{4}\pi$, $g_1(1\bar{1}0) = \frac{7}{16}\pi$, and $g_1(1\bar{1}1) = \frac{1}{2}\pi$.

II. \mathbf{B} Lying in a Plane Rotated Slightly from an (001) Plane: Geometry of Sample 58B

The orientation of sample 58B was rechecked by x-ray diffraction techniques after our frequency measurements had been completed. The current direction, originally thought to lie along an $[001]$ axis, was found to be rotated 8° away from the $[001]$ direction in the (110) plane. The transformation equations describing this orientation are obtained by the method outlined below.

A clockwise rotation around the k_z axis through an angle $\alpha (=45^\circ)$ is followed by a counterclockwise rotation around the k_x' axis through an angle $\beta (=8^\circ)$. Finally, a counterclockwise rotation is carried out around the k_z'' axis through an angle θ , where θ is the angle between the $[1\bar{1}0]$ direction (i.e., the k_x'' axis) and the magnetic field direction (which is now along the k_z''' axis). This sequence of rotations gives the following transformation equations:

$$\begin{aligned} k_x &= k_y''' (-\sin \theta \cos \alpha + \cos \theta \sin \alpha), \\ k_y &= k_y''' (\sin \theta \sin \alpha \cos \beta + \cos \theta \cos \alpha \cos \beta) \\ &\quad - k_z''' \sin \beta, \end{aligned} \quad (\text{A6})$$

$$k_z = k_y''' (\sin \theta \sin \alpha \sin \beta + \cos \theta \cos \alpha \sin \beta) + k_z''' \cos \beta,$$

where we have set $k_x'''=0$. A set of polar coordinates k_ρ and φ are introduced, where $k_y'''=k_\rho \cos \varphi$ and $k_z'''=k_\rho \sin \varphi$. Under the rotations described above, $f_1(\mathbf{k})$ may be written in the form $f_1(\mathbf{k}) = k_\rho^2 y_1(\theta, \varphi)$, where

where

$$p = (\Delta - E_0), \quad (\text{B2})$$

$$q = -(E_0 \Delta + k_F^2 P^2), \quad (\text{B3})$$

and

$$r = -\frac{2}{3} \Delta k_F^2 P^2. \quad (\text{B4})$$

The roots of Eq. (B1) are easily found by standard techniques.⁴⁰ Substituting for E' the value

$$E - \frac{1}{3} p, \quad (\text{B5})$$

⁴⁰ C. R. C. *Standard Mathematical Tables* (Chemical Rubber Publishing Co., Cleveland, 1957), p. 344.

Eq. (B1) is reduced to

$$E^3 + aE + b = 0, \quad (\text{B6})$$

where

$$a = \frac{1}{3}(3q - p^2) \quad (\text{B7})$$

and

$$b = (2p^3 - 9pq + 27r)/27. \quad (\text{B8})$$

Estimates of the band parameters establish the inequality $(\frac{1}{4}b^2 + a^3/27) < 0$; since this condition is satisfied, there will be three real and unequal roots of Eq. (B6) or, equivalently, of Eq. (B1). The roots are conveniently represented in trigonometric form. The roots of Eq. (B1) are

$$E_4' = (-\frac{1}{3}a)^{1/2} \cos \frac{1}{3}\varphi - \frac{1}{3}p, \quad (\text{B9})$$

$$E_1' = (-\frac{1}{3}a)^{1/2} \cos(120^\circ + \frac{1}{3}\varphi) - \frac{1}{3}p, \quad (\text{B10})$$

and

$$E_2' = (-\frac{1}{3}a)^{1/2} \cos(240^\circ + \frac{1}{3}\varphi) - \frac{1}{3}p, \quad (\text{B11})$$

where E_4' is the conduction-band solution of Eq. (B1), and E_1' and E_2' are the "split-off" and "low-mass" valence-band solutions of Eq. (B1), respectively. The value of the angle φ is calculated from the equation

$$\cos \varphi = -\frac{1}{2}b / (-a^3/27)^{1/2}. \quad (\text{B12})$$

Assuming the band parameters $\Delta = 0.80$ eV, $E_g = 0.81$ eV, and $P = 9.48 \times 10^{-8}$ eV cm, Eqs. (B2)–(B4), (B7)–(B9), and (B12) are used to calculate E_4' as a function of k_F . A plot of E_4' versus k_F^2 is shown in Fig. 11. The dashed straight line represents the initial slope of the curve and illustrates parabolic behavior.

The values of a_4 , b_4 , and c_4 are given by²²

$$a_4 = k_F P (E_4' + \frac{2}{3}\Delta) / N_1, \quad (\text{B13})$$

$$b_4 = \frac{1}{3}\sqrt{2}\Delta (E_4' - E_g) / N_1, \quad (\text{B14})$$

and

$$c_4 = (E_4' - E_g)(E_4' + \frac{2}{3}\Delta) / N_1, \quad (\text{B15})$$

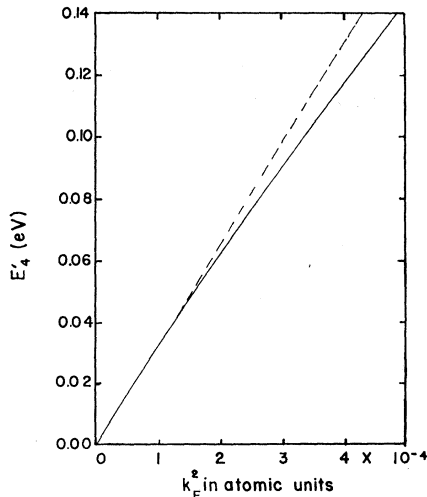


FIG. 11. Plot of E_4' versus k_F^2 ; the dashed line represents the initial slope and illustrates parabolic behavior.

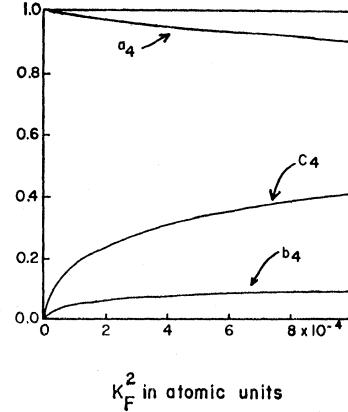


FIG. 12. Normalized coefficients for the Γ_6 conduction band of GaSb.

where N_1 is a normalizing coefficient determined by the relation

$$a_4^2 + b_4^2 + c_4^2 = 1. \quad (\text{B16})$$

Using the value of E_4' already determined and the band parameters listed previously, a_4 , b_4 , and c_4 can be calculated as a function of k_F . The dependence of a_4 , b_4 , and c_4 as a function of k_F^2 is shown in Fig. 12.

The appropriate spherical k_F for each sample is found by first determining the volume enclosed by the Fermi surface. The technique of Booth and Ewald³⁶ allows the volume to be expressed in terms of C_0 and C_1 . The volume can then be expressed as

$$V = \frac{4}{3}\pi C_0^{3/2} (1 - 0.2C_1). \quad (\text{B17})$$

In turn, k_F can be defined by

$$V \equiv \frac{4}{3}\pi k_F^3. \quad (\text{B18})$$

Thus

$$k_F \approx C_0^{1/2} (1 - 0.2C_1)^{1/3}. \quad (\text{B19})$$

APPENDIX C

In this appendix the details of a calculation to estimate the size of the higher-band parameter A' are presented.

In Sec. VI, Eq. (27) was used to determine a range of values of u (-2.1 to $+1.0$) corresponding to the uncertainty in the value of the Fermi energy of sample 80B. The value of C_0 used in Eq. (27) was accurately determined from our frequency data; in principle, it may be estimated from the Hall coefficient data or by some other experiment that measures the size of the Fermi volume. In the three higher-concentration samples used in this investigation, the Fermi energy lies above the $\langle 111 \rangle$ valley-band edge. Thus an estimate of C_0 from Hall-coefficient data involves a two-band analysis; the SdH effect gives C_0 directly.

Equation (13) can be used to estimate a value of the higher-band parameter A' , which is defined as the

matrix element sum

$$A' = -\frac{2}{m_0} \sum_j' \frac{|\langle s | p_x | u_j \rangle|^2}{(E_c - E_j)}, \quad (C1)$$

where the summation is over all states u_j transforming like Γ_{15} . The prime on the summation means that states in the four-dimensional subspace are not summed over. E_c is the energy of the Γ_1 state at the bottom of the conduction band. The x component of the momentum operator is represented by p_x , and s represents a function transforming like an atomic s function under the tetrahedral group. By using values of M and L' determined for InSb, we can estimate the values of $b_4^2 M$ and $c_4^2 L'$. The quantity M appearing in Eq. (13) is defined as

$$M \equiv H_1 + H_2, \quad (C2)$$

where H_1 is defined in Eq. (45) and

$$H_2 = -\frac{2}{m_0} \sum_j' \frac{|\langle x | p_y | u_j \rangle|^2}{(E_v - E_j)}. \quad (C3)$$

The Γ_{25} levels are expected to be far removed from Γ_{15} ,

and thus we consider $H_2 \approx 0$. The value of H_1 is not known for GaSb. In InSb, H_1 is of the order -5 .³¹ For the purpose of evaluating terms in u , we assume $H_1 \approx -5$, and therefore, $M \approx -5$. The quantity L' is defined as

$$L' \equiv F' + 2G, \quad (C4)$$

where

$$F' = -\frac{2}{m_0} \sum_j' \frac{|\langle x | p_x | u_j \rangle|^2}{(E_v - E_j)} \quad (C5)$$

and G was defined in Eq. (46). We assume that F' makes a negligible contribution to L' . In InSb, $G \approx -1$,³¹ and we adopt this value to estimate the size of L' . Thus, using Eq. (13), a value of $u = -2.1$ gives $A' \approx -3.2$; and $u = +1$ gives $A' \approx 0$. The magnitude of A' has not been previously determined experimentally in any semiconductors. Kane²² has suggested that A' is small compared to P^2/E_g . In the work of Groves *et al.*,⁴¹ the value of A' in HgTe has been taken as zero. Our estimates of A' based on SdH frequency data thus appear to be reasonable.

⁴¹ S. H. Groves, R. N. Brown, and C. R. Pidgeon, Phys. Rev. **161**, 779 (1967).

Donor-Acceptor Pair Lines in Cadmium Sulfide

C. H. HENRY, R. A. FAULKNER, AND K. NASSAU

Bell Telephone Laboratories, Murray Hill, New Jersey 07974

(Received 10 March 1969)

We report the first observation of donor-acceptor pair lines in CdS. The spectrum correlates with a distant pair peak at 5176 Å, an I_1 line at 4888.52 Å, and an I_2 line at 4869.30 Å. Several other pair-line spectra were observed in the vapor-grown undoped platelets used in these experiments. One of these correlated with the same I_1 line and distant pair peak, but with an I_2 line at 4869.17 Å. Zeeman experiments confirmed that these lines were donor-acceptor pair lines. The Zeeman pattern of the pair lines could be predicted, using a crystal field and a j - j coupling constant. These constants were determined by the splittings of the pair lines in zero field. For $\mathbf{H} \parallel c$, the hole g value was the same as for an isolated acceptor. A theoretical wurtzite spectrum was calculated on the basis of Coulomb interactions. The spectrum was much more complicated than a theoretical zinc-blende spectrum and was sensitive to both the dielectric-constant ratio $\epsilon_{II}/\epsilon_{II}$ and the c/a ratio of the CdS lattice. The experimental lines could not be assigned, but the line densities were in agreement with what was expected for a pair-line spectrum involving a simple donor and acceptor.

I. INTRODUCTION

THE edge emission in a semiconductor refers to the emission bands which occur with energies within a few tenths of an eV below the band gap.¹ Of all the II-VI semiconductors, the edge emission has been most extensively studied in CdS, where the

emission is in the blue and the green. The "blue edge" consists of sharp line emission from free and bound excitons and phonon replicas of these emission lines. Many of the prominent blue-edge emission lines have been classified by Thomas and Hopfield.² The most prominent of these are I_1 lines, which correspond to excitons bound to neutral acceptors, and I_2 lines, which correspond to excitons bound to neutral donors.

The "green-edge" emission in CdS consists of bands about 12-meV wide followed by a series of longitudinal

¹ Work on the edge emission in II-VI compounds has been reviewed by D. C. Reynolds, C. W. Litton, and T. C. Collins, Phys. Status Solidi **9**, 645 (1965); **12**, 3 (1965); R. E. Halstead, in *The Physics and Chemistry of II-VI Compounds*, edited by M. Aven and J. S. Prener (John Wiley & Sons, Inc., New York, 1967).

² D. G. Thomas and J. J. Hopfield, Phys. Rev. **128**, 2135 (1962).